Peertechz

ENGINEERING GROUP

Innovations in
Aerospace Science and Technology
OPEN ACCESS JOURNAL

DOI: https://dx.doi.org/10.17352/iast

Review Article

Feasibility of Martian Solar Powered Unmanned Aerial Vehicles in 2030s

Yrjö Jun Huang[1]* and Yinji Huang[2]

[1]Department of Aeronautics and Astronautics, Fudan University, Shanghai, China

[2]Shanghai TCab Technology Co. Ltd., China

Received: 16 June, 2025
Accepted: 23 June, 2025
Published: 24 June, 2025

***Corresponding author:** Yrjö Jun Huang, Department of Aeronautics and Astronautics, Fudan University, Shanghai, China, E-mail: jun_huang@fudan.edu.cn

Keywords: Aircraft on Mars; Feasibility; Solar powered; Fixed-wing aerial vehicles

https://www.engineegroup.com

Check for updates

Abstract

The exploration of Mars has been an aspiration since 1960s. The historical ways to explore Mars include orbiters, landers and rovers. Unlike the lunar exploration, aircraft on Mars can also be developed in the future, since the existence of Martian atmosphere. As a rising aerospace power, the idea of the Martian aircraft has also been proposed by many scholars. A solar-powered unmanned Martian airplane may be one such mission. However, compared with the Earth's environment, the Martian atmosphere is so rare and less predictable. In addition, the solar irradiance on Mars is weaker than that on the Earth. These are two uncertainties to the success of the development of such a Martian UAV (Unmanned Aerial Vehicle). In this article, the feasibility of this plan is discussed, based on the Martian environment, aerodynamic design and current technical reserves.

Nomenclature

Latin letters

A: Wing upper surface area, [m^2]; C_D: Drag Coefficient, [-]; C_L: Lift coefficient, [-]; E: Energy, [J]; F: Thrust, [N]; g: Gravitation, [m/s^2]; h: Altitude, [m]; I: Current, [A]; J: Power, [W]; j: Power on unit area, [W/m^2]; k: Atmosphere transparency, [-]; l: Chord of wing, [m]; m: Mass, [kg]; p: Pressure, [Pa]; Q: Martian daily solar irradiance, [J/(m^2·sol)]; q: Solar irradiance rate, [J/(m^2·s)]; R: Resistance, [Ω]; Re: Reynolds number, [-]; S: Area of solar cell, [m^2]; T: Temperature, [K]; t: Time, [s]; V: Voltage, [V]; u: Velocity, [m/s]

Greek letters

α: Lift-to-drag ratio, [-]; β: Bank angle, [°]; γ: Pitch angle, [°]; δ: Declination angle, [rad]; η: Lift drag ratio, [-]; θ: Efficiency coefficient, [°]; μ: Dynamics viscosity, [Pa·s]; ρ: Density, [kg/m3]; ρ: Mean density, [kg/m3]; χ: Mass-power ratio, [kg/kW]; τ: Constant, τ = 88,775.2, [s]; ψ: Martian latitude, [rad]; ω: Martian time angle, [rad]; $\omega*$: Sunrise and sunset times angle, [rad]

Superscripts and subscripts

A: Aircraft; b: Rechargeable battery; ctl: Control system; ext: Outside the Martian atmosphere; f: Fuel, propellant; g: Gear; i: Ignition; L: Lander; ls: Loss; m: Motor; o: Martian ground surface; p: Propeller; r: Rocket; s: Solar cell

Abbreviations

DGB: Disk-Gap-Band; EDL: Entry Descent Landing; HALE: High Altitude Long Endurance; GTO: Geocentric Orbits; JATO: Jet Assisted Take-Off; LEO: Low Earth Orbit; SPAMA: Solar Powered Automatic Martian Airplane; RAD: Rocket Assisted Descent; SL: Solar Longitude; TMI: Trans-Mars Injection; TOS: Take-Off Stand; UAV: Unmanned Aerial Vehicle; VTOL: Vertical Take-Off and Landing

1. Background

There have been several proposed missions to Mars

Citation: Huang YJ, Huang Y. Feasibility of Martian Solar Powered Unmanned Aerial Vehicles in 2030s. Innova Aerosp Sci Technol. 2025;3(1): 001-012.
Available from: https://dx.doi.org/10.17352/iast.000005

since 1960s [1]. All the missions can be classified into three groups, orbiters, landers and rovers. Among these plans, Mars 2020 by NASA is the one of the nearest plans. A robotic helicopter, Ingenuity, will help plan the best driving route for the rover. As the first unmanned Mars helicopter, it takes off from the ground and each flight lasts no more than 90 s, and the flight distance is around 300 m from the rover, at altitudes within 5 m above the ground. It is designed to use solar panels to recharge its batteries, and therefore the launch time is so limited, no more than once per Martian day [2-4].

On the other side, China is catching up on exploration of Mars. Tianwen-1 is such a mission to send a spacecraft to Mars, which includes an orbiter, a lander and a rover, named Zhurong [5]. Because of the shortages of the robotic helicopter, e.g. short flight time and short range, the feasibility of a Martian solar powered fixed-wing unmanned aerial vehicle is previewed, which is also abbreviated as SPAMA (Solar Powered Automatic Martian Airplane) for short. Not only fixed-wing aircraft, but also airship and sounding balloon can cover these shortages. Both of them have a large surface area to get enough solar energy. The stability and reliability of the airship and sounding balloon are better than those of fixed-wing aircraft, but the weight and volume of airship are fatal. Due to the low pressure of the Martian atmosphere, the volume of a solar powered Martian airship reaches at least 2×10^6 m^3 and the take-off mass is in 10 tons. The existing carrier rockets cannot complete a such heavy mission. In contrast, the smallest diameter of the Martian sounding balloon can be as small as 10 m, and the weight is less than 10 kg [6]. However, an unpowered sounding balloon has some disadvantages, too, e.g. uncontrollable and short working time. Of course, fixed-wing aircraft brings some other troubles, such as difficulties in take-off and landing, large size, requiring enough speed to generate sufficient lift force and so on. Fortunately, the recent development of solar powered High Altitude Long Endurance (HALE) aircraft gives a lot of reference for the design, e.g. Airbus Zephyr 8, the current record (26 days) for the longest non-stop unmanned solar powered aircraft [7]. Mozi II, as an improved version of Mozi, is a medium sized solar powered Unmanned Aerial Vehicle (UAV) with wingspan 15 m and aspect ratio 17.9 (Figure 1). It has the ability to fly in night after charging in sunlight, which is developed by a Chinese company, Oxai Aircraft. The authors (Huangs) and their students participated the solar powered aircraft project hosted by Oxai. Some ideas and designs about this aircraft are shown in this article.

Many scholars have also proposed the concept and design of Martian aircrafts [8-11], and even for other planets or satellites with an atmosphere, such as Venus and Titan [12,13]. This article is focused the feasibility of Martian aircrafts based on the existing technologies and the design

Figure 1: The Mozi solar powered UAV series:(a) Mozi and (b) Mozi II (photo by X.Fan)

concepts. But in the selection of technical parameters, some advanced data are selected.

The structure of this article is as follows: Sec. 2 is a general introduction to the Martian environment. In Sec. 3, the design and aerodynamic performance of the aircraft are introduced. The process and feasibility of rocket launching, capsule landing and aircraft take-off are introduced in Sec. 4. The last section is the conclusions.

2. Martian environment

The gravitation on Mars is weaker than that on the Earth due to the planets' smaller mass. The averaged free-air surface gravitational acceleration on Mars is 3.72 m/s^2, about 38% of that on the Earth, and it varies laterally. Generally speaking, the surface gravity of the two poles is higher and that near the equator is lower; the highest point, 3.743 m/s^2, is located near the Martian North Pole, while the lowest point 3.683 m/s^2 is located within the peaks in the Tharsis region. In addition, the gravitation decreases with altitude increasing [14]. Because the flying height of the SPAMA is not high and the difference of the surface gravitation is not large, the averaged value, g =3.72m/s^2, is used in the following calculations.

Sunlight is the main source of power for the SPAMA. Mars's average distance from the Sun is roughly 2.30×10^8 km, and its orbital period is 687 Earth days. A sol (Martian solar day) is about 24.6 hours, slightly longer than an Earth day. The orbital eccentricity of Mars is 0.093, which causes a large difference between the aphelion and perihelion distances (1.666 AU and 1.382 AU respectively), and the different lengths of each season. In order to obtain the

Citation: Huang YJ, Huang Y. Feasibility of Martian Solar Powered Unmanned Aerial Vehicles in 2030s. Innova Aerosp Sci Technol. 2025;3(1): 001-012.
Available from: https://dx.doi.org/10.17352/iast.000005

solar irradiance as much as possible, the working time of Mars Curiosity Rover was arranged when Mars is near the perihelion, namely Solar Longitude (SL) 251°. The planet during perihelion receives 40 percent more sunlight than during aphelion [15]. Mars's obliquity is 25.19°. Hence, the most suitable working place for the SPAMA might be slightly southerly to the equator. According to the data from Curiosity rover, which landed on Aeolis Palus (4.5°*S* and altitude *h* of -4.4 km). The surface daily solar irradiance keeps above 14 MJ/(m^2 sol) from SL 150° to 360° through a whole Martian year, if there no dust storm happens [16].

Martian dust storms are most common during perihelion. Observation since the 1950s has shown that the chances of a planet-wide dust storm in a particular Martian year are approximately 18-55% at the 95% level of confidence. The earlier observation indicates that great dust storms occur most frequently during southern spring and summer, or SL 160° ~ 315° and so called "dust storm season" [17,18].

The lift force of an aircraft is related to the characteristics of the surrounding atmosphere. It increases with the environmental pressure. The Martian atmosphere is primarily composed of CO_2 (95.3%), N_2 (2.6%) and Ar (1.9%) [19]. The mean molecular weight is 43.35, almost 50% higher than that of the Earth. While the viscosity of Mars atmosphere is around 1.3 × 10^{-5} Pa·s for density ρ = 0.02 kg/m^3. [20]. Compared to Earth's atmosphere, the wind circulation has a larger influence on the Martian atmosphere because of the stronger diurnal temperature contrast. In addition to being affected by altitude and latitude, the surface pressure has an obvious seasonal and daily periodicity. The approximate pressure variation range is between 650 Pa and 1000 Pa. There are two high pressure periods occur in summer and winter. The solar longitudes of these two periods are 30° ~ 90° and 210° ~ 330° respectively. In contrast, the latter has a higher pressure. Thus, the most suitable pressure period is staggered with that of solar irradiance. The meteorological data from Curiosity rover show the daily averaged pressure always keeps around 850 Pa and the daily fluctuation is less than 100 Pa, between 330° and 30° in SL. A

Martian atmosphere pressure model named after NASA Glenn is given by [21],

$$p = p_0 \times \exp(-0.9 \times 10^{-4} h), \quad (1)$$

where p_0 is the pressure on the surface and *h* is the altitude. In other words, the air pressure drops about 8.5% every 1000 m. This pressure is roughly equal to 32,000m above sea level on the Earth.

Temperature is another important state function. Near the landing site of Curiosity, the daily mean temperature is stable around 220 K~ 230 K between 150° and 30° in SL. Considering the daily fluctuation, it is between 185 K and 265 K. For low altitude less than 7000 m, the temperature can be calculated from the ground temperature, T_0, that [21],

$$T = T_0 - 9.98 \times 10^{-4} h. \quad (2)$$

Combined with the pressure formula, if the cruising altitude of an aircraft does not exceed 1000 m, the environmental pressure and temperature can be kept above 750 Pa and 260 K respectively. Following the ideal gas equation, the extremely low density is 0.0144 kg/m^3 when p = 730 Pa and T = 265 K. While, substituting the daily mean pressure, 780 Pa, and temperature, 225 K into the ideal gas equation, the mean density is obtained, that $\bar{\rho}_{air} = 0.0181\ \mathrm{kg/m^3}$. These two densities are located in the range of altitude, *h*, between 26,000 m and 28,000 m on the Earth using those different models summarized in ref [22]. It is lower than the world record for solar powered aircraft, 29,524 m, created by Helios Prototype [23]. Furthermore, the wind speed on Mars surface is close to that of the stratospheric on the Earth [24], except for the dust storm season. It keeps lower than 15 m/s throughout a Martian year, but can reach 50 m/s or higher in the dust storm season [16].

In conclusion, the environment on Mars is not friendly to aircrafts, including low pressure, weak sunlight and seasonal dust storms. After integrating these factors, the launch window is set between SL 330° and 345° (about 25 sols). The worst values and the means values of air density and pressure are given above. In the following calculation, compromised values are used, that ρ_{air}=0.016 kg/m^3 and p = 750 Pa. In addition, the minimum value of daily irradiance introduced above, Q =14 MJ / (m^2 sol), is employed [16].

3. Design

3.1 Aerodynamic configuration

The Martian aircraft mission has four goals: 1) launching an aircraft to the surface of Mars; 2) endurance of flight at least 10 sols (245 hours); 3) instruments loaded not less than 3 kg without power supply; and 4) the launch mission being arranged between 2030 and 2040. In combining the environment and launch capability, a scenario is presented. An imaginary working status is depicted in Figure 2. As shown in this figure, the aerodynamic configuration is the traditional single fuselage with canards. The canards can provide extra lift force to balance the pitching moment. Limited by the size of the payload fairing of the carrier rocket, the full wingspan is 15 m and length is 4.4 m. The details of the carrier rocket will be presented in Subsection 4.1. A large aspect ratio rectangular wing can increase both the glide ratio and the area for solar cell. In this design, the aspect ratio is set around 10. The other details in size are

Citation: Huang YJ, Huang Y. Feasibility of Martian Solar Powered Unmanned Aerial Vehicles in 2030s. Innova Aerosp Sci Technol. 2025;3(1): 001-012.
Available from: https://dx.doi.org/10.17352/iast.000005

presented in Figures 3,4. The airfoil is LINDNER2, which produces a high lift coefficient for Reynolds number **Re**~ 6 × 10^5. Here, the Reynolds number is defined by **Re**= $\rho l u_A/\mu$, in which u_A is 25 m/s (90 km/h), chord or wing l is 1.5 m, density ρ = 0.02 kg/m^3 and viscosity μ is 1.3 × 10^{-5} Pa·s [20]. A large designed speed u_A may increase the lift force, but it also increases drag force and required engine power. Figure 5 depicts the drag and lift coefficients of the airfoil LINDNER2 near this Reynolds number.

Although we follow some experience from the design of Mozi II, the dual fuselage structure in Mozi II is given up. The low gravity on Mars can reduce the strength requirement. On the other hand, the aircraft needs more space to arrange the rechargeable batteries to meet the night flight. In the design shown in Figures 2,3, the internal volume of the fuselage is 40 L. The lowered nose staggers the heights of the canards and wings to reduce aerodynamic interference between them.

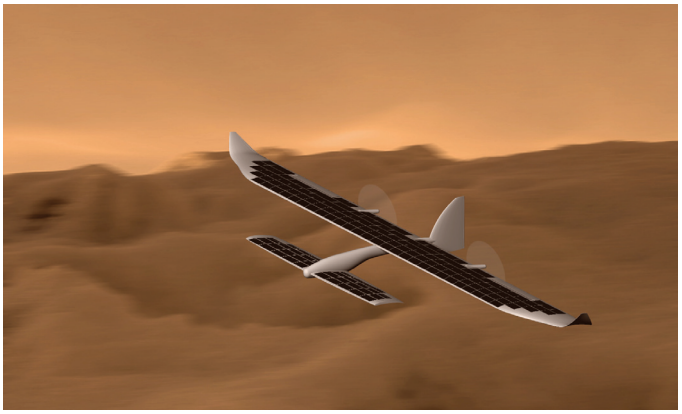

Figure 2: 3D Design Rendering.

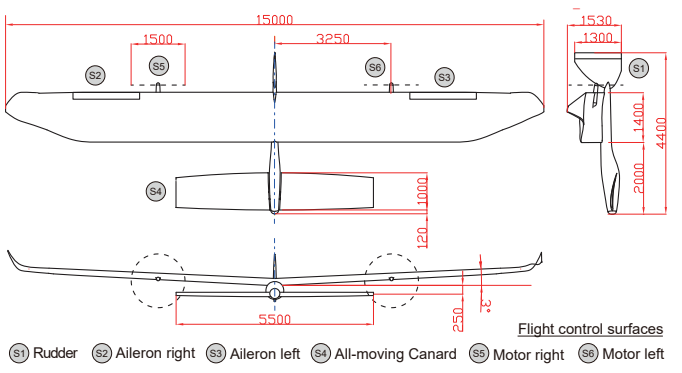

Figure 3: Three view plan of the SPAMA and flight control surfaces.

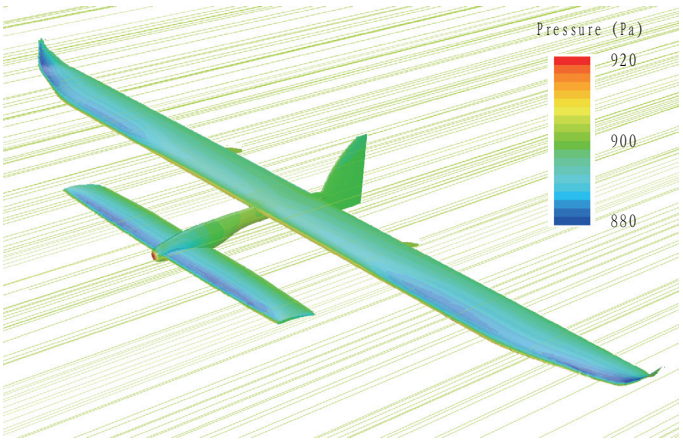

Figure 4: Pressure distribution on the surface of the Martian UAV and streamlines near the aircraft from CFD simulation for pitch angle γ = 2°.

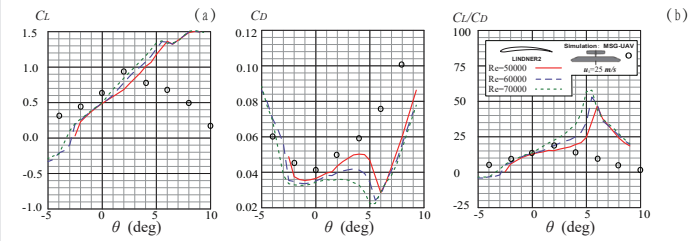

Figure 5: Aerodynamic characteristics (a) Lift coefficient C_L vs. attack angle, θ; (b) Lift coefficient C_D vs. θ and (c) lift-drag ratio C_L/C_D, or α vs. θ. Here, lines are for the airfoil, LINDER2, and circles are for the SPAMA. The airfoil is presented in the upper-right corner of subfigure (c).

As the last part of this subsection, the aerodynamic performance of the whole SPAMA is simulated through CFD analysis. Most of these numerical simulations were carried out by using Star-CCM+. A nested unstructured mesh is used in this simulation with a minimum cell size of 1 cm near the leading edge of the propeller and the wings. The total number of grids in the nested mesh is around 88,000 and $k-\omega$ model is used in this simulation. The flow field and coefficients are presented in Figures 4,5 respectively. The installation angle of the wing causes the lift coefficients curve left-shift. It can be seen that when the attack angle is within the range of $-2^\circ < \theta < 4^\circ$, the lift-to-drag ratio remains above 10. While the SPAMA flies horizontally, namely pitch angle $\gamma = 0^\circ$, the lift-drag ratio reaches 18.2. Here, the attack angle and the pitch angle are equal, because the air is approaching horizontally. In our calculation, the lift-drag ratio is set as α = 15. Finally, because of weight reduction, solar panel area, flight mission and flight altitude, etc., only the basic control surfaces are installed, as shown in Figure 3.

3.2 Power and engine

The low-density atmosphere on Mars may easily lead to laminar flow separation for propellers, which leads to a rapid decrease in drag coefficient. On the other hand, in order to ensure thrust, the diameter and speed of the propeller have to be large enough; this further intensifies laminar-flow separation. Therefore, multi-propeller configuration is commonly used for those high-altitude solar powered aircrafts to avoid laminar flow separation. Currently, the high-efficiency propeller designs and applications for the stratosphere of the Earth's atmosphere above 20 km are widely carried out. Colozza introduced their propeller performance curves for a 2 bladed propeller at altitudes

Citation: Huang YJ, Huang Y. Feasibility of Martian Solar Powered Unmanned Aerial Vehicles in 2030s. Innova Aerosp Sci Technol. 2025;3(1): 001-012.
Available from: https://dx.doi.org/10.17352/iast.000005

of 24-31 km [25]. With the increase in altitude, the thrust drops from 10 N to 4 N, and the power drops from 1750 W to 625 W; while the efficiency rises from 84% to 93%. The Helios Prototype is powered by 14 brushless direct-current electric motors. These motors are rated at 2 hp. (1.5 kW) each, and drive lightweight two-blade propellers of 79-inch diameter. The efficiency of these propellers is 80% at an altitude of 27 km [26]. According to these two examples, the expected efficiency of the propeller, η_p is set as 0.8 in our calculation.

As shown in Figure 2, only solar panels are installed on the upper surface of the wings and canards. The approximate area of solar cells, S, can reach $17m^2$, about 73% coverage. The solar-powered aircraft, Mozi II, is equipped with 10 m^2 gallium arsenide (Ge-Ar) thin film solar cell. The cell type is multijunction solar cell assembly on Ge substrate. The manufacturer of the solar cell claimed the averaged efficiency can be 30% or even higher, which is very close to the world record of thin-film solar cells produced in lab [27]. But in fact, the averaged measured efficiency is around 20% in normal weather. This difference may be caused by many factors, such as temperature, load, light intensity, incident angle, etc. Generally speaking, the higher light intensity, the higher energy conversion efficiency is. The sunlight on Mars is weaker than that on the Earth, so the efficiency of this solar cell should be even lower. Additionally, the cold temperature on Mars may also affect the efficiency of solar cell. Since this launch mission is designed for ten years later, a reasonable but slightly over-estimated efficiency is used in calculations.

Moreover, some other technical operations, such as flying in the opposite direction of rotation in daytime and slight tilting caused by the cooperation among the control surfaces, increase the solar energy reception by 5% or more. According to the previously estimated daily solar irradiance Q =14 MJ/(m^2 sol) and 20% conversion efficiency of the solar cell η_s, the total electrical energy being generated throughout a whole sol is given by,

$$\begin{aligned} E_S &= Q \cdot S \cdot \eta_S \cdot \left(1 + \eta_t\right) \\ &= 14\ \text{MJ} / \left(\text{m}^2 \cdot \text{sol}\right) \times 17\ \text{m}^2 \times 20\% \times \left(1 + 5\%\right) \\ &= 49.98\ \text{MJ}. \end{aligned} \tag{3}$$

In other words, the average power throughout the whole sol is the total energy E_s divided by a Martian solar day in second, τ = 24h39′35.2” = 88,775.2 s,

$$J_S = \frac{E_s}{\tau} = 563\text{W}, \tag{4}$$

and the power per unit area of solar cell $j_s = J_s/S$ = 31.5 W/m^2. While the average propulsion power required is given by,

$$\begin{aligned} J_p &= \frac{m_A u_A g}{\alpha(\eta_m \eta_{ctl} \eta_p)\eta_b} \\ &= \frac{60\ \text{kg} \cdot 25\ \text{m/s} \cdot 3.72\ \text{m/s}^2}{15 \times 77\% \times 90\%} \\ &= 537\ \text{W}, \end{aligned} \tag{5}$$

where m_A is the mass of the SPAMA, η_p, η_m, η_{ctl} and η_B are the efficiencies of the propeller, motor, control system and battery charging respectively. Noth listed the efficiencies of eight HALE aircrafts [11]. The products of η_m, η_{ctl} and η_p vary from 0.68 to 0.84. Here, the median value is selected, that $\eta_m\eta_{ctl}\eta_p$ = 0.77. The difference between J_s and J_p can be used for avionics, control surfaces and other loads. According to the value of J_p, it can be estimated that the minimum power consumption (without loads) in a whole sol is 48 MJ.

3.3 Weight and structure

Weight control is one of the key technologies in design of a Martian aircraft. As already mentioned in Sec.3.2, the total mass of the aircraft is set as 60 kg. The estimated weight of each item is listed in Table 1. The basis for each main item is presented as follows:

- **Solar cell:** The 20% photoelectric conversion efficiency of solar cell mentioned before is a relatively high value selected. If the photoelectrical conversion efficiency cannot be effectively improved, then an increase in the efficiency-to-weight ratio becomes the only direction. We have a similar solar cell to that used by Mozi II, with a unit weight of approximately 0.3kg/m^2. This weight includes base material, bypass diode, anti-reflective coating, interoceptors and cover-film. The potential of weigh reduction is not too much. Compared with the Earth, Mars has lower solar irradiance and longer nighttime and therefore, additional solar cell is required. As a result, the total mass of the solar cell increases proportionally, and the mass m_s, is, $\rho_s S$ = 0.3 kg/m^2×17 m^2=5.1 kg ≈ 5 kg.
- **Rechargeable battery:** The solar irradiance rate on Mars, q, varies with the declination angle δ, Martian time angle ω, latitude ψ, and atmospheric transparency k, which can be written as [15]:

Table 1: Mass of the SPAMA components.

Item	kg
solar cell	5
rechargeable battery	17
main structure	30
propulsion system	1
avionics	2
load	3
others	2
Total	< 60

Citation: Huang YJ, Huang Y. Feasibility of Martian Solar Powered Unmanned Aerial Vehicles in 2030s. Innova Aerosp Sci Technol. 2025;3(1): 001-012.
Available from: https://dx.doi.org/10.17352/iast.000005

$$q = q_{ext} k\left[\sin\delta\sin\psi + \cos\delta\cos\psi\cos\omega\right](q \geq 0), \tag{6}$$

where q_{ext} is the solar irradiance of the outside the atmosphere. The atmospheric transparency k is affected by many parameters, such as air quality, density, and angle of incidence. To simplify the problem, both q_{ext} and k are assumed as constants. The landing date and place of landing have been discussed in Sec.2. Substituting $\delta = 15^\circ$ and $\psi = 4^\circ$ into this formula, it can be approximated as:

$$q = q_{ext} k\cos\omega \ (q \geq 0). \tag{7}$$

This curve is plotted in Figures 6,7. Then, the total electrical power supply from the solar cell is given by,

$$E_S = 2kq_{ext}\eta_b S\int_0^{\frac{\pi}{2}}\cos\omega d\omega = 48 \text{ MJ} \tag{8}$$

Converting the time angle ω to time t in second leads to,

$$E_S = 2kq_{ext}\eta_b S\int_0^{\frac{\tau}{4}}\cos\frac{2\pi t}{\tau}dt = 48 \text{ MJ} \tag{9}$$

Then, kq_{ext} = 450 W by solving this equation. When $\omega^* = \pm 0.4\pi$, the charging and discharging are balanced. Hence, at least 60% of the electricity, namely E_s = 29 MJ, needs to be reserved for the night. Generally speaking, the efficiency of solar cells is very low at dawn or dusk, so it is necessary to choose a large safety margin, η_m. Here, the safety margin is set as 20%. In addition, the energy loss in discharging process also should be added. Bernardi et al. presented a general energy balance for battery systems [28]. In his model, the energy loss is composed of five parts: electrical heat, reactions, phase changes, mixing and heat transfer with the surroundings. Among these five terms, the first term plays the main role, and therefore, the energy loss can be written as,

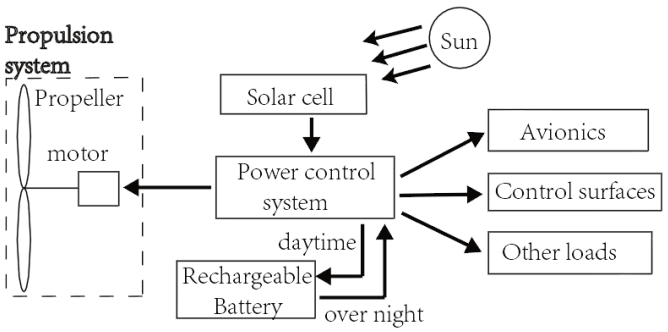

Figure 6: Structure diagram of power system in the SPAMA.

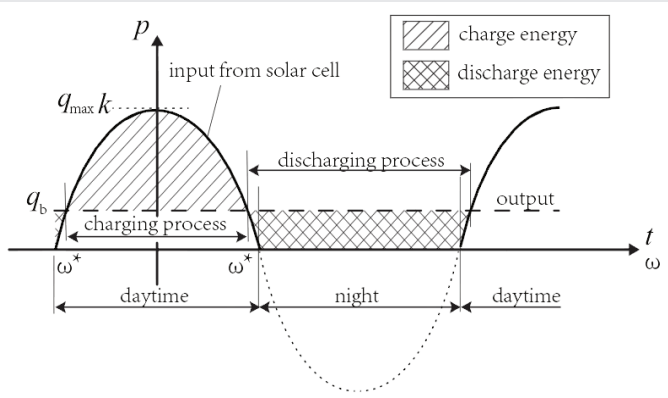

Figure 7: Energy balance diagram of the SPAMA.

$$E_{ls} = \frac{I^2 \cdot R}{V}. \tag{10}$$

In this equation, V is voltage, R is battery internal resistance, I is current. The current I is positive when discharging, while it is negative when charging. In this case, the charge and discharge currents are roughly the same, and therefore, the energy loss can be approximately set as 1 − 50%η_b = 5%. The capacity of the battery can be calculated by,

$$E_b = \frac{(1+\eta_m)E_S}{(1-\eta_b)} = 36.7\text{MJ}. \tag{11}$$

A lot of new type of high energy density rechargeable batteries have been developed recently in response to the future market, such as lithium-sulfur battery (Li-S battery), magnesium battery, metal (lithium, aluminum, zinc) air batteries, etc., The Zephyr 7 broke a world record for the longest duration as a solar powered unmanned aircraft in 2010, lasting 14 days. The energy density of the Li-S battery produced by Sion Power reached 375 Wh/kg [29]. The theoretical energy density of Li-S batteries is about 2600 Wh/kg. It has already achieved over 400 Wh/kg in commercial-size pouch cells [30]. Today, some non-commercial packed Li-S batteries or hydrogen fuel cell batteries (including the hydrogen and oxygen storage cylinders) reaches the level of 600 Wh/kg. Of course, considering the working temperature and discharge rate, this value may be lower [31]. It should be noticed that the new record in laboratory is as high as 1675 Wh/kg, almost 65% of the theoretical value. Even after 60 cycles of charging and discharging, the performance drops by about 40% to 1050 Wh/kg. Magnesium-sulfur (Mg-S) battery is another interesting candidate. The Mg/Mg^{2+} redox couple provides almost double the volumetric capacity than Li Here, setting the energy density at 600 Wh/kg is a reasonable value.

The total mass of the rechargeable battery can be roughly calculated by,

$$\begin{aligned} m_b &= \frac{E_b}{J \times 3600 \text{ s}} \\ &= (3.7 \times 107 \text{ J})/(600 \text{ Wh/kg} \times 3600 \text{ s}) \\ &= 16.95 \text{ kg} < 17 \text{ kg}. \end{aligned} \tag{12}$$

This is the basic requirement for level flight. Control and navigation require extra power, so the total mass of the

Citation: Huang YJ, Huang Y. Feasibility of Martian Solar Powered Unmanned Aerial Vehicles in 2030s. Innova Aerosp Sci Technol. 2025;3(1): 001-012.
Available from: https://dx.doi.org/10.17352/iast.000005

rechargeable battery is set as 18 kg in Table 1. Generally, the specific density of the Li-S battery is between 1 and 1.5 kg/L, so the volume does not exceed 18 L, which is enough to be placed in the fuselage.

By the way, in addition to the battery, there is another energy storage technology for solar powered aircrafts, that converts the potential energy of the flight altitude into kinetic energy. Usually, 20% to 30% of the energy can be stored in this way. But for the Martian aircraft, the low gravity environment and insufficient flight altitude make this ratio much lower. Finally, low temperatures may adversely affect battery efficiency, but they can also increase atmospheric density, which is beneficial for flight. The battery itself also generates heat during operation. In addition, proper insulations and preheating measures can effectively mitigate the impact of low temperatures on the battery.

- **Structure:** Composite materials are a good choice for structural applications, where high stiffness-to-weight and strength-to-weight ratios are required. Aircrafts are typically weight sensitive structures in which composite materials can be cost-effective [32]. In order to meet the requirements of long-term flight, solar powered HALE aircrafts are usually made of full composite materials. Mozi II, which has a take-off weight around 70 kg (including 7 kg payload), more than 50% of which are composite materials for the frames and skin. Because the gravity on Mars is much lower than that on the Earth, the strength of the structure can be appropriately reduced. Compared with the four engine nacelles and dual-fuselage of Mozi II, the two engine nacelles and single-fuselage design can also effectively reduce weight. To further reduce weight, no landing gear is installed; therefore the aircraft does not need an airstrip. When the power is not enough, the craft crashes. In addition, due to the size limitations of the launch vehicle, some designs of Martian aircraft use foldable wings and fuselage [11]. Such a kind of design requires additional mechanical components and weight to meet strength requirements. Considering the size of the carrier rocket, an integrated fuselage and wing is adopted to reduce weight. Finally, more advanced materials or technologies can also be used to improve the weight of the aircraft structure. For example, multi-functional structural energy-storage composite materials can not only store energy but also act as structural materials. Based on the above reasons, setting the structure weight at 30 kg is achievable.

- Propulsion system: As shown in Sec.3.2, the propulsion system is composed of three subparts, control electronics, motor, and propeller. Noth sorted out the mass-power ratios of these subparts used on solar powered aircraft, and found that they are almost constants [11]. Eq.5 gives the engine output in level flight, J_p, is 537 W. If the continuous maximum power, $P_{p,max}$, is approximated as double of P_p, namely $P_{p,max}$ = 1100 W, then the total mass of motors and controller is given by,

$$\begin{aligned} m_p &= \left(\chi_{ctl} + \chi_m + \chi_p + \chi_g\right) P_{p,max} \\ &= \left(0.026 + 0.3 + 0.25 + 0.2\right) \text{kg/kW} \times 1.1 \text{ kW} \\ &= 0.85 \text{ kg} \approx 1.0 \text{ kg} \end{aligned} \quad (13)$$

- **Miscellaneous:** Other weights include load, avionics and so on. Generally speaking, weak electric appliances are not heavy. However, the weight of the cable between the battery, motor and the solar cell cannot be ignored. Probably the most effective solution is to use high voltage, low current, and small wire diameter to achieve weight reduction. According to our experience, the total weight of a UAV of such size (incl. cable) can be controlled within 3 kg. The last row of the table, "Others", can be used as a safety margin to allocate weight distribution.

4. EDL (Entry, descent and landing) and take-off

4.1 Carrier rocket

As of 2020, the Long March V (also known as Changzheng V, CZ-5 and LM5,) is the heaviest, and most powerful rocket series in China. Six CZ-5 variants were originally planned, but only two of them were launched, as shown in Figure 8, base variant based on CZ-5D & CZ-5E, and low Earth orbit (LEO) variant based on CZ-5B [33,34]. It is emphasized here that the final sequence and configuration are slightly different from this plan. The new plan has not been deciphered yet, and only this plan that has been verified for technical feasibility can be discussed here. The maximum payload capacities of CZ-5E are about 25,000 kg to Low Earth Orbit (LEO), 14,000 kg to Geostationary Transfer Orbit (GTO) and 6000 kg to Mars transfer orbit, commonly known as Trans-Mars Injection (TMI). The sizes of the payload fairings are shown in Figure 9. The payload

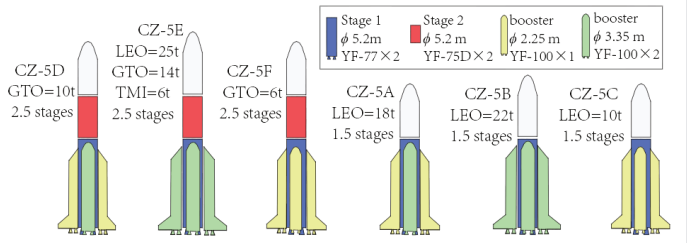

Figure 8: Long March V (Changzheng-5) series.

Citation: Huang YJ, Huang Y. Feasibility of Martian Solar Powered Unmanned Aerial Vehicles in 2030s. Innova Aerosp Sci Technol. 2025;3(1): 001-012.
Available from: https://dx.doi.org/10.17352/iast.000005

fairing for CZ-5B is composed of two halves and each half weighs 1,740 kg. [35,36]. Compared with CZ-5D, the planned variant CZ-5E has a higher carrying capacity and a longer fairing, about 19 m. The size of the Martian aircraft is tailored to the size of the fairing.

In addition to the CZ-5E, the Long March IX (also known as Changzheng 9, CZ-9 and LM-9,) series with diameter of 9.5 m is also a candidate launch vehicle. However, CZ-9 is currently in the research and development stage, and it is expected to be launched for the first time near 2030 [37]. Until now, we do not have too many details about it yet, so the discussion is only based on the CZ-5E as the launch vehicle.

4.2 Landing capsule

The sketch of the landing capsule in the landing state is presented in Figure 10. With reference to some other Mars landers, Figure 11 presents a rough landing plan. In short, the landing capsule is separated from the cruise capsule near the altitude of 6000 km and enters the landing phase. The descending process includes three phases, aerodynamic deceleration, parachute deceleration and reverse thrust deceleration, as shown in this figure. In this process, the fairing and the parachute system and are sequentially jettisoned, to reduce the load of the parachute and the Rocket Assisted Descent (RAD) system. Finally, a soft landing is achieved on the surface of Mars. As introduce above, the payload carrying capacity of the launch vehicle, CZ-5E, is 6,000 kg. However, due to that of the parachute descent system, the total mass entering Martian atmosphere is controlled less than 5,800 kg. The weight of each main item is roughly planned as shown in Table 2, and more details will be carried as follows. If the optional loads shown in Figure 10 are not included, the weight can be further reduced to around 5500 kg.

- **Payload fairing:** Usually, the payload fairing is used to protect a spacecraft payload against the impact of dynamic pressure and aerodynamic heating during launch through an atmosphere. Once outside the atmosphere of Earth, the fairing is jettisoned, reducing the load and exposing the payload to outer space. However, the Martian atmospheric entry also causes mechanical stress and aerodynamic heating to the landing capsule. Thus, the fairing will be kept until the landing deceleration phase in Martian atmosphere.

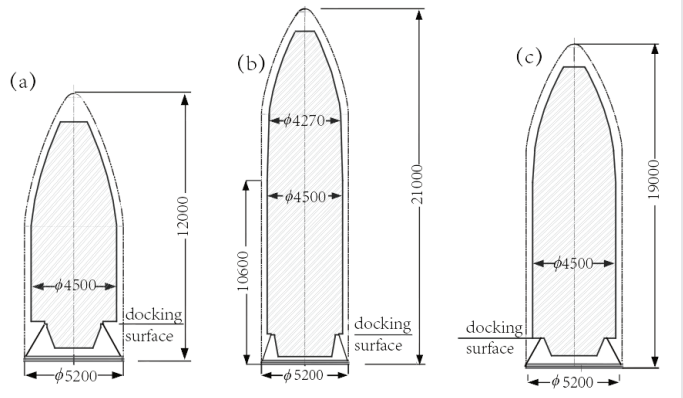

Figure 9: Payload fairings used in CZ-5 series: (a) CZ-5D, (b) CZ-5B, and (c) extended fairing for CZ-5E.

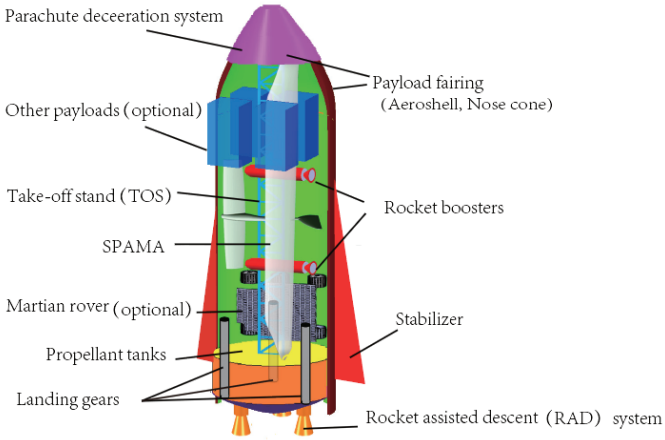

Figure 10: Sketch of the landing capsule.

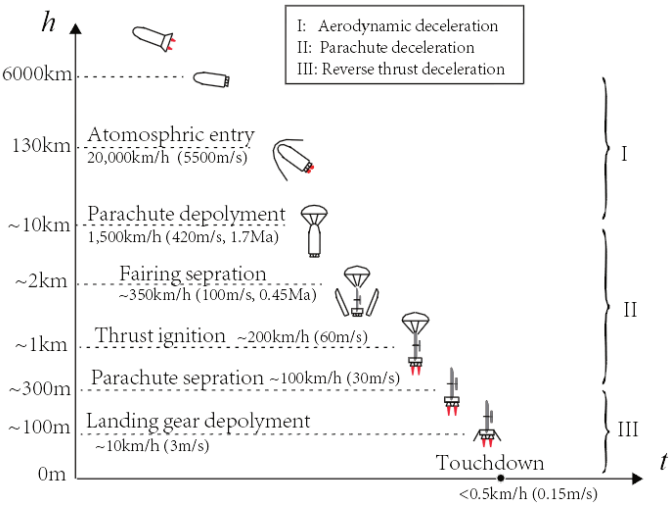

Figure 11: Entry, Descent, and Landing (EDL) Sequence.

Table 2: Weight of the landing capsule components.

Item	
payload fairing (incl. stabilizer)	< 3500
propellant for entry	~ 600
propellant for landing	~ 350
RAD system	~ 200
parachute deceleration system	~ 200
TOS and other mechanical structures	200
control and power system	100
SPAMA and rocket boosters	100
other optional items	300 – 600
Total	< 5800

Citation: Huang YJ, Huang Y. Feasibility of Martian Solar Powered Unmanned Aerial Vehicles in 2030s. Innova Aerosp Sci Technol. 2025;3(1): 001-012.
Available from: https://dx.doi.org/10.17352/iast.000005

The parameters of the CZ-5 series payload fairings are introduced above. By analogy, the weight of the fairing in this mission (Figure 9(c)) is about 3,500 kg, which becomes the largest component of the mass of the landing capsule, m_L. It should be noticed that this weight includes the stabilizer. The stabilizer can not only provide lift force to extend the deceleration time, but also reduce rolling and maintain the stability of the landing capsule in aerodynamic deceleration phase. It makes the aerodynamic deceleration process similar to that of space shuttles [38] or the recovery process of the first stage of Falcon 9. When the first-stage engines are shut down, Falcon 9 is travelling at Mach 10 (~3 km s^{-1}) at an altitude of 80 km [39]. Due to inertia, it can eventually rise to a height of 140 km [40]. Because the scale height of the Martian atmosphere is around 1.2-1.4 times of the Earth's atmosphere, the atmospheric conditions here should be similar to the Martian atmosphere near 60-80 km. The data from the recovery process may provide some engineering information for future missions to the payload landing.

Different from Falcon 9, a rough attitude adjustment is only required in the entry stage. In addition, the gravity of Mars is much lower than that of the Earth, namely fuel consumption is also lower. It is estimated that 10% of the total weight, about 600 kilograms of propellant is needed for entry stage.

- **Parachute descent system:** A large supersonic Disk-Gap-Band (DGB) parachute operated successfully on Mars and helped the Curiosity rover landing in 2012, with 150 kN (34,580 lb) peak inflation load at a Mach number Ma=1.7 [41]. The largest ever parachute will land Europe's ExoMars in 2021. This ring-slot parachute is 35 m across and weigh almost 90 kg and the landing module is about 2000 kg [42,43]. Tanner, et al. introduced two large Martian parachutes [44]. The larger one is designed for landing module of 3000 kg at the range of Mach 1.6–2.1. The mass of this parachute decelerator system is 125 kg, and its peak load for inflation load reaches 420 kN (90,700 lb). Obviously, this parachute is overloaded in this SPAMA mission. Here, three solutions are given:

1. Further increasing the size of the parachute in diameter. This solution is a great challenge to the material.

2. Using two to three parachutes in series. Usually, a parachute reaches its peak load occurs after 2 to 4 seconds of being deployed. Therefore, the difficulty in this solution is the timing control.

3. Reducing the speed to 1.3 Ma in the end of the aerodynamic deceleration phase. The stabilizer shown in Figure 10 generates lift force at a large attack angle, and it may extend the aerodynamic deceleration time, to achieve the purpose of further deceleration.

- **RAD system:** The RAD system is essential for a safe landing on Mars. Without the RAD retrorocket engines, the Mars lander would hit the ground at high speed. Some parameters about RAD systems of previous Mars landers are listed in Table 3, including mass of landers and propellants, thrusts, ignition times, etc., [45–52]. All the RAD systems listed in this table use similar hydrazine propellant, so the difference in specific impulse shouldn't be too much. Except for Curiosity, the others are finally landing with airbag, which can reduce the propellant consumption and impact. It should be noticed that the mass in the table is the total mass that enters the Martian atmosphere; According to Table 2, the mass of the final soft-landing part in our mission is no more than 2,000 kg, only about one third of the total mass in Table 2. 15% is a conservative valuation for the mass ratio of m_f/m_L, namely 300 kg propellant for landing stage.

If the total thrust is set at about 20 kN, three YF-50D engines in parallel may be a good candidate. For each of them, the thrust is up to 6.5 kN, the specific impulse is 315, and the propellant consumption rate is about 2 kg/s. The following equation can be used to estimate the minimum ignition time in RAD phase, that is

$$m_E \cdot g \cdot t_i + m_E \cdot u_E = F \cdot t_i. \quad (14)$$

Substituting the mass of lander m_E = 2200 kg, velocity near the end of Parachute phase u_E =60 m/s, and the total thrust F=6.5 kN × 3=19.5 kN into this equation, the solution of ignition time t_i = is 11.7 s, and the total propellant consumption is 70 kg. It shows that the 750 kg propellant is indeed a conservative estimate.

At present, China already has the rocket vertical landing technology. In October 2021, Dark Blue Aerospace, a private aerospace enterprise in China, completed a vertical take-off and landing (VTOL) flight using their liquid propellant rocket, Nebula-M. The highest point of the trajectory is

Table 3: Parameters related to RAD in some Martian landers.

Project (unit)	*mL* (kg) †	*mf* (kg)	*Mf*/ *mL*	*F*(N)	t_i(s)
Mars Polar Lander	494	64	13.0%	3,192	40
Phoenix	600	64	10.7%	3600	40
Curiously	2401	387	16.1%	13,200	40+12 ‡
Mars Pathfinder	584	94	16.1 %	7,938	22
Viking	992	85	8.6 %	7,800	-

†Total mass of entering atmosphere, incl. all parts separated in midway.
‡Landing by sky crane. 40s for descent & touchdown; 12s for sky crane flyaway.

Citation: Huang YJ, Huang Y. Feasibility of Martian Solar Powered Unmanned Aerial Vehicles in 2030s. Innova Aerosp Sci Technol. 2025;3(1): 001-012.
Available from: https://dx.doi.org/10.17352/iast.000005

103.2 m. At the state level, the Long March 8 series (CZ-8) is a new generation of medium-sized and low orbit two-stage launch vehicle and the carrying capacity for GTO is around 2.5 tons. Two commercial launches have been completed by February 2022. The VTOL model of the CZ-8 series is CZ-8R. [53] Thus, the final touchdown becomes relatively simple. In addition to the RAD phase, the retrorockets in the RAD system are also ignited during the aerodynamic deceleration phase to adjust the attitude, but the output is much lower than that of the Reverse thrust deceleration phase.

4.3 Take-off

Compared with the EDL process, the Martian aircraft take-off is much easier. Since there is no landing gear, booster rockets would be used, which is called Jet Assisted Take-Off (JATO). Before take-off, the aircraft is fixed on a Take-off Stand (TOS). It is a bar in a mechanical linkage, which can change the bank angle of the aircraft. In the reverse thrust deceleration, the bank angle of the aircraft is 90°, as shown in Figure 11. Another role of the TOS is linking the parachute system, the RAD system and the other parts of the lander after the payload fairing being separated. While the bank angle becomes 0° by rotating the TOS, before the aircraft's take-off. If a Martian rover is equipped, the rover can also be fixed to the TOS, and be released using rope, or tilting the TOS.

The two rocket boosters should be ignited at the same time, as the thrust of solid booster usually uncontrollable, the control surface is only way to balance attitude. This requires an advanced flight control technology. Another solution is to take off with multirotor and then abandon the rotors will all attachments. At present, the third author's company is developing a pure electric VTOL manned aircraft, and their technology may help for this solution.

4.4 Avionics system

Avionic systems include communications, navigation, flight control and so on. There is no doubt that satellite system is a good choice for communications and navigation. Since the flight area does not cover the whole Mars, Compared with

GPS, the number of satellites is much reduced. Secondly, satellites are launched from the Earth, the cost for high orbit satellite are almost the same as that for lower orbit satellite. This will also help reduce the number of satellites. With reference to the first phase of Beidou (Beidou-1), an experimental regional satellite navigation system in 2000, four geostationary orbit satellites (three working satellites and one backup satellite) serviced from longitude 70°E to 140°E and from latitude 5°N to 55°N [54] (Figure 12).

In addition to the satellite system, the azimuth of the sun in daytime, the position of the stars in night, camera and radar are also helpful in navigation.

5. Conclusion

This article presents a plan of Martian solar powered fixed-wing UAV. Combining our experience in solar powered HALE aircraft and some existing technologies, the feasibility of this Martian UAV is discussed from a mechanical view. Here, some parameters selected are higher than the current technical level, but can be reached in the near future, such as solar cell efficiency and energy storage density, etc. Through the calculation, it shows such a Martian UAV is an achievable plan in the future.

There are several bottlenecks in the existing technical reserves. For aircraft, two main bottlenecks are the efficiency of solar cell and the capacity of the rechargeable batteries, if the lift-drag ratio, α, cannot be greatly improved. In contrast, the improvement of solar cell is limited, and the potential of rechargeable batteries may be greater. On the other hand, although the aerodynamic configuration shown in this article can provide a large lift-drag ratio, and a large wing surface area for more solar cell, the control robustness is not high. If there is improvement in the power system, the aerodynamic configuration can also be further optimized. In addition, the EDL process of the lander on the surface of Mars is also a difficult problem. No such huge object has landed on Mars yet. But some recent technologies, such as high-capacity Li-S battery, HALE UAV on the Earth, Mars rover landing, and space shuttle return, show that it not far from technological breakthroughs.

In addition to these bottlenecks, the environment on Mars is more fatal, such as the ultra-low atmospheric pressure, weak solar irradiance, significant changes in altitude, and periodic Martian dust storms. In this article, the sunlight intensity used is 14 MJ/(m^2·sol), and the solar cell efficiency is 20%. In theory, the efficiency of a multi-junction gallium arsenide cell reaches 50%. It can be seen that the solar irradiance rate within 30 degrees north-south latitude remains 8 MJ/(m^2·sol) or higher throughout the Martian year, except for dust storm season [16]. If both the efficiency of solar cell and the mass power ratio of battery

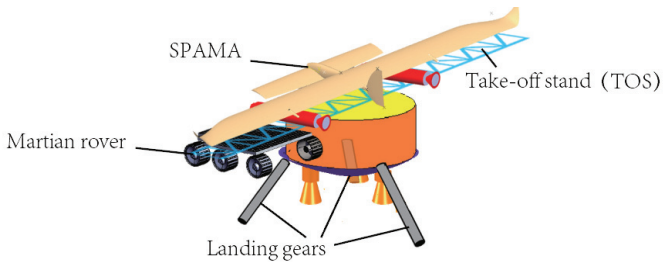

Figure 12: Take-off state.

Citation: Huang YJ, Huang Y. Feasibility of Martian Solar Powered Unmanned Aerial Vehicles in 2030s. Innova Aerosp Sci Technol. 2025;3(1): 001-012.
Available from: https://dx.doi.org/10.17352/iast.000005

can be increased by 50% or more, the flight can be more than half a year until the solar cell or the battery aging or a dust storm coming.

In the beginning of the article, the bottleneck and shortages of Martian airship and Martian sounding balloon are also listed. At the current stage, sounding balloons may be the most reliable, the highest cost-effective and easiest way to explore the Martian atmosphere, although it has some disadvantages such as uncontrollable and short flight time. But the Martian aircraft may be a better option in the future.

Acknowledgement

The first author obtained financial support from Fudan University and National Natural Science Foundation of China (No.12273004). The authors thank CFD software Star-CCM+ provided by CD-adapco (Siemens PLM Software) and Mandy Guo's technical support.

References

1. Szocik K. Is human enhancement in space a moral duty? missions to Mars, advanced AI and genome editing in space. Cambridge Quarterly of Healthcare Ethics. 2020;29(1):122–30. Available from: https://doi.org/10.1017/s0963180119000859

2. Young LA, Delaune J, Johnson W, Withrow S, Cummings H, Sklyanskiy E, et al. Design Considerations for a Mars Highland Helicopter. In: ASCEND 2020. 2020. p. 4027. Available from: https://doi.org/10.2514/6.2020-4027

3. Schroeder G. NASA's Ingenuity Mars Helicopter: The first attempt at powered flight on another world. American Scientist. 2020;108(6):330–1. Available from: https://go.gale.com/ps/i.do?id=GALE%7CA640622186&sid=googleScholar&v=2.1&it=r&linkaccess=abs&issn=00030996&p=AONE&sw=w&cookieConsent=true&analyticsOptout=false&userGroupName=anon%7E8777bd43&aty=open-web-entry

4. Farley KA, Williford KH, Stack KM, Bhartia R, Chen A, de la Torre M, et al. Mars 2020 mission overview. Space Science Reviews. 2020;216(8):1–41. Available from: https://link.springer.com/article/10.1007/s11214-020-00762-y

5. Peng Y, Zhang L, Cai Z, Wang Z, Jiao H, Wang D, et al. Overview of the Mars climate station for Tianwen-1 mission. Earth and Planetary Physics. 2020;4(4):371–83. Available from: http://dx.doi.org/10.26464/epp2020057

6. Kerzhanovich V, Cutts J, Cooper H, Hall J, McDonald B, Pauken M, et al. Breakthrough in Mars balloon technology. Advances in Space Research. 2004;33(10):1836–41. Available from: http://dx.doi.org/10.1016/j.asr.2003.05.023

7. d'Oliveira FA, Melo FCLd, Devezas TC. High altitude platforms present situation and technology trends. Journal of Aerospace Technology and Management. 2016;8(3):249–62. Available from: http://dx.doi.org/10.5028/jatm.v8i3.699

8. Liu T, Oyama A, Fujii K. Scaling analysis of propeller-driven aircraft for Mars exploration. Journal of aircraft. 2013;50(5):1593–604. Available from: http://dx.doi.org/10.2514/1.C032086

9. Guynn M, Croom M, Smith S, Parks R, Gelhausen P. Evolution of a Mars airplane concept for the ARES Mars scout mission. 2nd AIAA Unmanned Unlimited Conf. and Workshop & Exhibit. 2003. p. 6578. Available from: https://ntrs.nasa.gov/api/citations/20040034201/downloads/20040034201.pdf

10. Kwiek A. Conceptual design of an aircraft for Mars mission. Aircraft Engineering and Aerospace Technology. 2019;9. Available from: http://dx.doi.org/10.1108/AEAT-08-2018-0231

11. NOTH A. Design of solar powered airplanes for continuous flight [PhD thesis]. ETH ZÜRICH; 2008. Available from: https://www.research-collection.ethz.ch/bitstream/handle/20.500.11850/14994/eth-31170-01.pdf

12. Colozza A. Feasibility of a long duration solar powered aircraft on Venus. In: 2nd International Energy Conversion Engineering Conference. 2004. p. 5558. Available from: https://doi.org/10.2514/6.2004-5558

13. Barnes JW, Lemke L, Foch R, McKay CP, Beyer RA, Radebaugh J, et al. AVIATR aerial vehicle for In-situ and airborne Titan reconnaissance. Experimental Astronomy. 2012;33(1):55–127. Available from: https://ntrs.nasa.gov/api/citations/20140011539/downloads/20140011539.pdf

14. Hirt C, Claessens S, Kuhn M, Featherstone W. Kilometer-resolution gravity field of Mars: MGM2011. Planetary and Space Science. 2012;67(1):147–54. Available from: https://ddfe.curtin.edu.au/models/MGM2011/Hirt2012_MGM2011.pdf

15. Appelbaum J, Flood DJ. Solar radiation on Mars. Solar Energy. 1990;45(6):353–63. Available from: https://ntrs.nasa.gov/api/citations/19910005804/downloads/19910005804.pdf

16. Mart´ınez G, Newman C, De Vicente-Retortillo A, Fischer E, Renno N, Richardson M, et al. The modern near-surface Martian climate: A review of in-situ meteorological data from Viking to Curiosity. Space Science Reviews. 2017;212(1-2):295–338. Available from: https://link.springer.com/article/10.1007/s11214-017-0360-x

17. Zurek RW, Martin LJ. Interannual variability of planet-encircling dust storms on Mars. Journal of Geophysical Research: Planets. 1993;98(E2):3247–59. Available from: https://doi.org/10.1029/92JE02936

18. Kass D, Kleinb¨ohl A, McCleese D, Schofield J, Smith M. Interannual similarity in the Martian atmosphere during the dust storm season. Geophysical Research Letters. 2016;43(12):6111–8. Available from: https://ui.adsabs.harvard.edu/link_gateway/2016GeoRL..43.6111K/doi:10.1002/2016GL068978

19. Trainer MG, Wong MH, Mcconnochie TH, Franz HB, Atreya SK, Conrad PG, et al. Seasonal variations in atmospheric composition as measured in Gale Crater, Mars. Journal of Geophysical Research: Planets. 2019;124(11):3000–24. Available from: https://doi.org/10.1029/2019JE006175

20. Almeida MP, Parteli E, Andrade JS, Jr, Herrmann HJ. Giant saltation on mars. Proceedings of the National Academy of Sciences of the United States of America. 2008;105(17):6222–6. Available from: https://doi.org/10.1073/pnas.0800202105

21. Zuppardi G. Influence of the Mars atmosphere model on aerodynamics of an entry capsule. Adv. Aircraft Spacecraft Sci. 2019;6(3):239–56. Available from: https://doi.org/10.12989/aas.2019.6.3.239

22. Qu W-J, Zhu W-Y, Song S-L, Ping J-S. Evaluation of the precision of three tropospheric delay correction models. Chinese Astronomy and Astrophysics. 2008;32(4):429–38. Available from: https://ui.adsabs.harvard.edu/link_gateway/2008ChA&A..32..429Q/doi:10.1016/j.chinastron.2008.10.010

23. Sener E, Turk I, Yazar I, Karakoc TH. Solar powered UAV model on MATLAB/Simulink using incremental conductance MPPT technique. Aircraft Engineering and Aerospace Technology. 2019;92:93-100. Available from: http://dx.doi.org/10.1108/AEAT-04-2019-0063

24. Drob DP, Emmert JT, Meriwether JW, Makela JJ, Doornbos E, Conde M, et al. An update to the Horizontal Wind Model (HWM): The quiet time thermosphere. Earth and Space Science. 2015;2(7):301–19. Available from: http://dx.doi.org/10.1002/2014EA000089

25. Colozza AJ. APEX 3D propeller test preliminary design. 2002. Available from: https://ntrs.nasa.gov/citations/20020082943

Citation: Huang YJ, Huang Y. Feasibility of Martian Solar Powered Unmanned Aerial Vehicles in 2030s. Innova Aerosp Sci Technol. 2025;3(1): 001-012. Available from: https://dx.doi.org/10.17352/iast.000005

26. Noll TE, Ishmael SD, Henwood B, Perez-Davis ME, Tiffany GC, Madura J, et al. Technical findings, lessons learned, and recommendations resulting from the helios prototype vehicle mishap. National Aeronautics and Space Admin Langley Research Center Hampton Va; 2007. Available from: https://ntrs.nasa.gov/citations/20070022260

27. Green MA, Dunlop ED, Levi DH, Hohl-Ebinger J, Yoshita M, Ho-Baillie AW. Solar cell efficiency tables (version 54). Progress in photovoltaics: research and applications. 2019;27(7):565–75. Available from: https://doi.org/10.1002/pip.3171

28. Bernardi D, Pawlikowski E, Newman J. A general energy balance for battery systems. Journal of the electrochemical society. 1985;132(1):5. Available from: https://ui.adsabs.harvard.edu/link_gateway/1985JEIS..132....5B/doi:10.1149/1.2113792

29. Brooks P. High-Altitude, Long-Endurance Unmanned Aerial Vehicles (HALE UAVs)–A Perfect First Application for Lithium–Sulfur Batteries. Lithium-Sulfur Batteries. 2019. Available from: https://doi.org/10.1002/9781119297895.ch12

30. Dong T, Peng P, Jiang F. Numerical modeling and analysis of the thermal behavior of NCM lithium-ion batteries subjected to very high Crate discharge/charge operations. International journal of heat and mass transfer. 2018;117:261–72. Available from: https://doi.org/10.1016/j.ijheatmasstransfer.2017.10.024

31. Osada I, von Zamory J, Paillard E, Passerini S. Improved lithiummetal/vanadium pentoxide polymer battery incorporating crosslinked ternary polymer electrolyte with N-butyl-N-methylpyrrolidinium bis (perfluoromethanesulfonyl) imide. Journal of Power Sources. 2014;271:334–41. Available from: https://doi.org/10.1016/j.jpowsour.2014.08.019

32. Vasi´c Z, Maksimovi´c S, Georgijevi´c D. Applied integrated design in composite UAV development. Applied Composite Materials. 2018;25(2):221–36. Available from: https://link.springer.com/article/10.1007/s10443-017-9611-y

33. Li D, Li PQ, Wang J, Huang B, Liu B. General scheme and key technologies of long march 5 launch vehicle (in chinese). Journal of Deep Space Exploration. 2021;8(4):335–43.

34. Qin T, Xu L, Liu J. Development of China's new generation launch vehicles. Chinese Journal of Space Science. 2018;38:593–7. Available from: https://dx.doi.org/10.15982/j.issn.2096-9287.2021.20210009

35. Ai S. Separation simulation studies of large-scale payload fairing [Master's thesis]. Dalian Univ. Tech.; 2015.

36. Li PQ, Li D, Yang HJ, Huang B, Huang H. Development and application analysis and future prospect of lm-5 series launch vehicles (in chinese). Missiles and Space Vehicles. 2021;379(2):5–16.

37. Cai T. A new generation of launch vehicle in Zhuhai Airshow, Long March 9 heavy rocket in development (in Chinese). Aerospace China. 2008;11:29–31.

38. Jenkins DR. Space Shuttle: Developing an Icon: 1972-2013. Specialty Press; 2016. p. 1584. Available from: https://books.google.co.in/books/about/Space_Shuttle.html?id=DaYBMQAACAAJ&redir_esc=y

39. NASA. Spacex crs-6 mission-cargo resupply services mission, press kit. 2015. Available from: https://www.nasa.gov/wp-content/uploads/2018/07/spacex_nasa_crs-6_presskit-2.pdf

40. Seedhouse E. SpaceX's Dragon: America's Next Generation Spacecraft. Springer; 2015. Available from: https://content.e-bookshelf.de/media/reading/L-8071876-29b9af8fbb.pdf

41. Cruz JR, Way D, Shidner J, Davis JL, Powell RW, Kipp D, et al. Reconstruction of the Mars Science Laboratory parachute performance and comparison to the descent simulation. In: AIAA Aerodynamic Decelerator Systems (ADS) Conference. 2013. p. 1250. Available from: https://ntrs.nasa.gov/citations/20130012763

42. Barrett A. Where should the ExoMars rover land? Astronomy & Geophysics. 2018;59(5):5–12. Available from: https://doi.org/10.1093/astrogeo/aty229

43. Pultarova T. The Largest Parachute Ever Built for Mars Aces Its First Test. 2018. Available from: https://www.space.com/40597-giant-mars-parachute-passes-first-test.html

44. Tanner CL, Clark IG, Chen A. Overview of the Mars 2020 parachute risk reduction activity. In: 2018 IEEE Aerospace Conference. 2018;1–11. Available from: http://dx.doi.org/10.1109/AERO.2018.8396717

45. Spencer DA, Blanchard RC, Braun RD, Kallemeyn PH, Thurman SW. Mars Pathfinder entry, descent, and landing reconstruction. Journal of Spacecraft and Rockets. 1999;36(3):357–66. Available from: https://doi.org/10.2514/2.3478

46. NASA. 1998 Mars Missions - NASA's Mars Exploration Program. 1998. Available from: https://mars.nasa.gov/internal_resources/818/

47. NASA. Mars Science Laboratory Landing Press Kit. 2012. Available from: https://www.jpl.nasa.gov/news/press_kits/MSLLanding.pdf

48. NASA. Mars exploration rover launches. 2003. Available from: https://www.jpl.nasa.gov/news/press_kits/merlaunch.pdf

49. Barber T, Picha F. In-flight propulsion system characterization for both Mars Exploration Rover spacecraft. In: 40th AIAA/ASME/SAE/ASEE Joint Propulsion Conference and Exhibit. 2004;3695. Available from: https://ntrs.nasa.gov/citations/20060046320

50. NASA. Viking Mission to Mars, NASA Facts. 2003.

51. NASA. Mars Pathfinder, NASA Facts. Available from: https://mars.nasa.gov/internal_resources/815/

52. Braun RD, Manning RM. Mars exploration entry, descent and landing challenges. In: 2006 IEEE Aerospace Conference. 2006;18. Available from: https://ntrs.nasa.gov/citations/20060050781

53. Song ZY, Wu YT, Xu S, Chen X, Xiao Y. Lm-8: the pioneer of long march rocket series on the innovations of commercialization and intelligence (in chinese). Journal of Deep Space Exploration. 2021;8(1):3–16. Available from: https://dx.doi.org/10.15982/j.issn.2096-9287.2021.20200009

54. Yang Y, Tang J, Montenbruck O. Chinese navigation satellite systems. In: Springer Handbook of Global Navigation Satellite Systems. 2017;273–304. Available from: https://link.springer.com/chapter/10.1007/978-3-319-42928-1_10

Citation: Huang YJ, Huang Y. Feasibility of Martian Solar Powered Unmanned Aerial Vehicles in 2030s. Innova Aerosp Sci Technol. 2025;3(1): 001-012. Available from: https://dx.doi.org/10.17352/iast.000005